THE JOURNAL OF PHYSICAL CHEMISTRY C

Article

pubs.acs.org/JPCC

Symmetry-Breaking Charge Transfer of Visible Light Absorbing Systems: Zinc Dipyrrins

Cong Trinh,[†] Kent Kirlikovali,[†] Saptaparna Das,[†] Maraia E. Ener,[‡] Harry B. Gray,[‡] Peter Djurovich,[†] Stephen E. Bradforth,[†] and Mark E. Thompson*[,†]

[†]Department of Chemistry, University of Southern California, Los Angeles, California 90089, United States

[‡]California Institute of Technology, 1200 East California Boulevard, Pasadena, California 91125, United States

Supporting Information

ABSTRACT: Zinc dipyrrin complexes with two identical dipyrrin ligands absorb strongly at 450−550 nm and exhibit high fluorescence quantum yields in nonpolar solvents (e.g., 0.16−0.66 in cyclohexane) and weak to nonexistent emission in polar solvents (i.e., $<10^{-3}$, in acetonitrile). The low quantum efficiencies in polar solvents are attributed to the formation of a nonemissive symmetry-breaking charge transfer (SBCT) state, which is not formed in nonpolar solvents. Analysis using ultrafast spectroscopy shows that in polar solvents the singlet excited state relaxes to the SBCT state in 1.0−5.5 ps and then decays via recombination to the triplet or ground states in 0.9−3.3 ns. In the weakly polar solvent toluene, the equilibrium between a localized excited state and the charge transfer state is established in 11−22 ps.

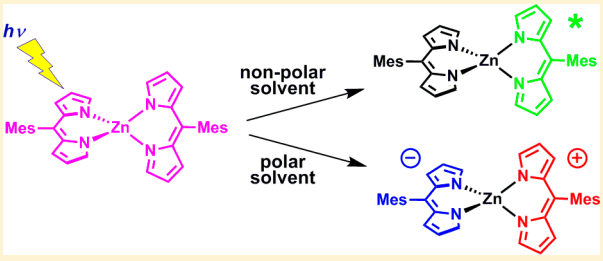

INTRODUCTION

Photoinduced charge transfer (CT) via symmetry breaking (SB) plays a crucial role in photosynthetic reaction centers in living systems.[1−8] These systems contain two or more virtually identical and symmetric chromophores. CT from one chromophore to another occurs upon photoexcitation, producing SB charge separation. Of great potential interest, but less well explored, are SBCT processes in organic photovoltaics (OPV) and related solar-harvesting systems.[9−21] Among well-documented simple organic compounds exhibiting SB phenomena are 9,9′-bianthryl derivatives;[22−30] however, they do not absorb visible light, making them of limited use in systems harvesting the solar energy. Indeed, very few organic dyes that absorb in the visible region undergo SBCT processes.[8,31−35] Herein, we investigate the photophysics of zinc dipyrrin complexes (Figure 1) that exhibit intense visible absorption in a range of organic solvents. These compounds have structural features related to 9,9′-bianthryl (i.e., poorly coupled orthogonal chromophores) that are conducive to photoinduced SBCT processes in weakly polar to polar solvents. Zinc dipyrrins and analogous compounds are attractive because, in addition to strong absorption in the visible region of the spectrum, their syntheses are easy and scalable. Moreover, the large body of work on boron dipyrrins (bDIP) can be used to guide ligand design.[36,37]

In OPVs, the low dielectric constants of organic materials ($\varepsilon_s \approx 3$) lead to high exciton binding energies, and thus, a large energy offset between donor and acceptor is required to promote charge generation at the donor/acceptor interface (D/A).[38] Use of organic dyes that undergo SBCT processes might be a potential solution to reduce the energy cost for exciton dissociation to free charges at D/A. The polar environment at D/A may be sufficient to induce SBCT in the chromophore, leading to spontaneous formation of internal CT excitons. Charge separation between electron donor and acceptor materials from these SBCT excitons is expected to proceed

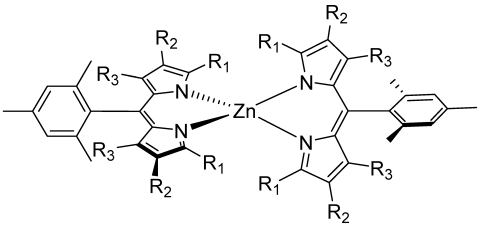

zDIP1: $R_{1\text{-}4}$ = H; ***zDIP3***: $R_{1,3}$ = -CH_3, R_2 = H
zDIP2: R_1 = -CH_3, $R_{2,3}$ = H; ***zDIP4***: $R_{1,3}$ = -CH_3, R_2 = -C_2H_5

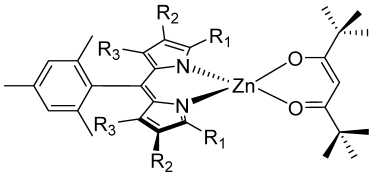

zDIP2′: R_1 = -CH_3, $R_{2,3}$ = H; ***zDIP3′***: $R_{1,3}$ = -CH_3, R_2 = H

Figure 1. Structures of homoleptic (zDIP1−zDIP4) and heteroleptic (zDIP2′ and zDIP3′) zinc dipyrrin complexes.

Received: July 9, 2014
Revised: August 27, 2014
Published: August 27, 2014

with lower energetic requirements than for typical Frenkel excitons found in organic materials. That being the case, the ability of zinc dipyrrin complexes to undergo SBCT makes them a potential family of new materials for use in organic photovoltaics.

Fluorescent metallodipyrrins have attracted considerable attention due to their potential use as probes for sensing metal ions (in particular, Zn^{2+}) in living systems.[39,40] However, in spite of the increasing number of reported metallodipyrrins,[37,41−51] their photophysics are not well-understood. Unlike the highly fluorescent bDIPs,[36,37] homoleptic complexes MD_n (D = dipyrrin or π-extended dipyrrin ligands)[43,44,46,47,49] generally exhibit low to moderate fluorescent quantum yields. In contrast, the heteroleptic complexes MDX_n (X is an ancillary ligand) were shown to have quite high luminescent efficiencies (up to 80%).[41−45,50,51]

Several nonradiative deactivation pathways have been suggested for the photoinduced excited state of homoleptic zinc dipyrrins and π-extended dipyrrins. Lindsey and coworkers reported that rotation of the phenyl ring at the meso-position on the dipyrrin ligand is a source of nonradiative deactivation of the excited state.[47] Replacement of phenyl with the more bulky mesityl substituent to form zDIP1 inhibits this rotation, leading to an improved quantum yield of 36% in toluene.[47] Interestingly, a recent study on related mesityl-substituted zinc dipyrrins (zDIP2 and zDIP4) has reported that the quantum yields of the homoleptic complexes are strongly dependent on solvent polarity, decreasing from 20−30% in toluene to ≤5% in dichloromethane.[44] The authors proposed that this decrease in polar solvents is due to thermal promotion from a locally excited state on a single dipyrrin ligand to a nonemissive, charge-separated state (i.e., D^+-Zn-D^-);[44] however, no additional photophysical data was provided to support this hypothesis. Strong excitonic coupling between nonorthogonal ligands has also been suggested as another nonradiative deactivation pathway of zinc π-extended dipyrrin complexes.[43] However, excitonic coupling[52,53] between the nearly orthogonal ligands in homoleptic zinc dipyrrin compounds such as zDIP2 and zDIP4 is negligible[54,55] and thus cannot be used to explain the decrease in luminescent efficiency compared to their heteroleptic counterparts. In this paper, we show that SBCT in polar solvents is an effective nonradiative decay pathway for the electronic excited states of homoleptic zinc dipyrrins. In nonpolar solvents such as cyclohexane, these complexes do not undergo SBCT and thus exhibit even higher quantum yields than their heteroleptic analogs.

EXPERIMENTAL SECTION

The synthesis and characterization by NMR, mass spectroscopy, and elemental analysis of the zinc dipyrrin complexes described here are given in the Supporting Information (SI) for this paper.

Electrochemical and Photophysical Characterization. Cyclic voltammetry (CV) and differential pulse voltammetry (DPV) were performed using an EG&G Potentiostat/Galvanostat model 283. Freshly distilled THF (VWR) was used as the solvent under inert atmosphere with 0.1 M tetra(*n*-butyl)ammonium hexafluorophosphate (Aldrich) as the supporting electrolyte. A glassy carbon rod, a platinum wire, and a silver wire were used as the working electrode, counter electrode, and pseudoreference electrode, respectively. Electrochemical reversibility was established using CV, while all redox potentials were determined using DPV and are reported relative to a ferrocenium/ferrocene (Fc^+/Fc) redox couple used as an internal standard. A scan rate of 100 mV/s was used for all measurements.

The UV−visible spectra were recorded on a Hewlett-Packard 4853 diode array spectrophotometer. Steady-state emission experiments at room temperature and 77 K were performed using a Photon Technology International QuantaMaster model C-60SE spectrofluorometer. Fluorescence lifetimes were determined through time-correlated single-photon counting methods. Fluorescence lifetime measurements in cyclohexane, toluene, and THF were performed using an IBH Fluorocube instrument equipped with a 405 nm LED excitation source with the IRF value of 0.4 ns. Fluorescence lifetime measurements in dichloromethane and acetonitrile were carried out using an excitation wavelength of 500 nm obtained from an optical parametric amplifier (Coherent OPA 9450) pumped by a 250 kHz Ti:sapphire amplifier (Coherent RegA 9050). The emission was collected at 520 nm for S_1 state and 645 nm for the CT state using a R3809U-50 Hamamatsu PMT with a Becker and Hickl SPC 630 detection module (22 ps time resolution). Quantum efficiency measurements were carried out using a Hamamatsu C9920 system equipped with a xenon lamp, calibrated integrating sphere, and model C10027 photonic multichannel analyzer. The error in the emission lifetime measurements is ±5% and for the quantum yields is ±10%.

Femtosecond Transient Absorption. Pump and probe pulses were obtained from the output of a Ti:sapphire regenerative amplifier (Coherent Legend, 1 kHz, 4 mJ, 35 fs). The excitation pulses centered at 500 nm were generated by pumping a type-II OPA (Spectra Physics OPA-800C) with ∼10% of the amplifier 800 nm output and mixing the resulting OPA signal output with the residual 800 nm pump in a type-II BBO crystal. White light supercontinuum probe pulses spanning the visible (320−950 nm) were obtained by focusing a small amount of the amplifier output into a rotating CaF_2 disk. The supercontinuum probe was collimated and focused with a pair of off-axis parabolic mirrors into sample, whereas the pump was focused before the sample position using a 25 cm CaF_2 lens. To avoid any contribution to the observed dynamics from orientational relaxation, the polarization of the supercontinuum was set at the magic angle (54.7°) with respect to the pump polarization. The cross-correlation between pump and probe in a thin 1 mm quartz substrate gave a fwhm of 180 fs for 500 nm excitation. The supercontinuum probe was dispersed using a spectrograph (Oriel MS127I) onto a 256-pixel silicon diode array (Hamamatsu) for multiplexed detection of the probe.

Samples containing zDIP1, zDIP2, or zDIP3 dissolved in cyclohexane, toluene, dichloromethane, or acetonitrile were placed in a closed, capped 1 mm quartz cuvette. The concentration of each sample was adjusted to give an optical density between 0.11 and 0.18 at 500 nm. The solutions were deaerated by bubbling with N_2 prior to analysis. During data collection, the samples were slowly oscillated perpendicular to the pump and probe to reduce photodamage to the sample by the pump. At early time delays, a strong nonresonant signal from the sample cell and solvent is observed. The solvent response is found to relax within 180 fs for cyclohexane, dichloromethane, and acetonitrile, while in toluene this signal was stronger and obscured the first 300 fs. To effectively remove this nonresonant signal, a second measurement of the

Scheme 1. Synthesis of (a) zDIP1−zDIP4 and (b) zDIP2′ and zDIP3′ Complexes

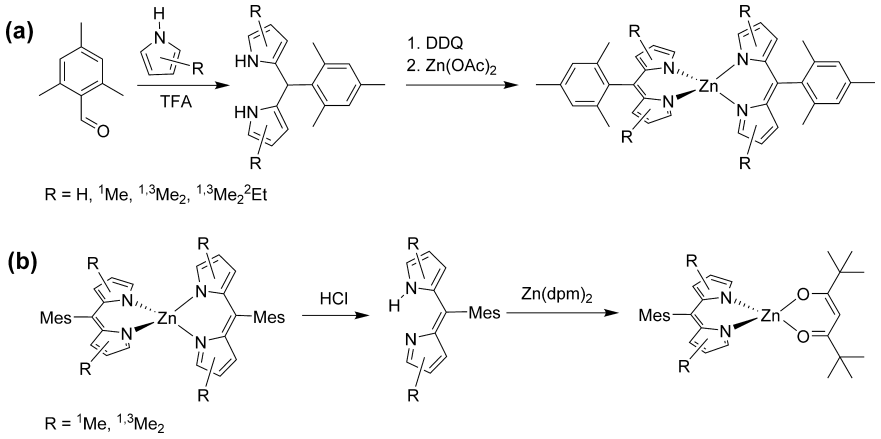

neat solvent was performed in an identical cuvette under same excitation conditions. The transient signal resulting from the solvent was then subtracted from the zinc dipyrrin solution signal. The nonresonant solvent response did, however, give a useful measure of the temporal dispersion of the supercontinuum after propagating through the CaF_2 plate and sample. The presented data have been corrected to account for this dispersion. Transient absorption measurements were performed with pump fluences varying between 70 and 300 $\mu J/cm^2$. Over this range, the signal was found to scale linearly with the pump energy.

Nanosecond-to-Millisecond Transient Absorption. Samples were prepared in a nitrogen glovebox with dry solvents, such that the maximum absorbance was approximately OD = 1. These samples were sealed in 1 × 1 cm^2 quartz cuvettes with Kontes valves to keep the solution air-free. The third harmonic of a 10 Hz Q-switched Nd:YAG laser (Spectra-Physics Quanta-Ray PRO-Series, pulse width: 8 ns) was used to pump an optical parametric oscillator (Spectra-Physics Quanta-Ray MOPO-700), tunable in the visible region. The excitation wavelength for each sample was chosen such that OD (at λ excitation) = 0.3−0.4, and the laser power was attenuated to 3 mJ/pulse using a half-wave plate and polarizer combination. For single-wavelength transient absorption kinetics measurements, probe light was provided by a 75 W arc lamp operated in either continuous or pulsed mode. Single wavelengths were selected by a double monochromator with 1 mm slits, detected by a photomultiplier tube, and amplified and recorded with a transient digitizer. Single-wavelength traces were acquired at approximately 5 nm increments over the range of 350−595 nm, on a 2 μs, 100 μs, or 10 ms timebase window, averaging over 300 laser pulses. A reference wavelength (400 nm) was acquired as every third trace, to take into account the photodegradation of the sample. Data were converted to units of $\Delta OD = -\log_{10}(I/I_0)$. Kinetics traces at each wavelength were scaled on the basis of the intensity of the previous reference trace. Decays were fit to a single or double exponential with a long-time offset using Matlab (version 2010b) curve fitting software. To generate transient absorption profiles at various time points, the ΔOD at that time point was taken from the exponential fit of each single-wavelength kinetics trace.

Single Crystal Crystallography. The X-ray crystal structures of zDIP3, zDIP4, zDIP2′, and zDIP3′ were determined using a Bruker APEX II CCD system equipped with a TRIUMPH curved-crystal monochromator and a Mo Kα fine-focus tube (λ = 0.710 73 Å). The frames were integrated with the Bruker SAINT software package using a SAINT V7.68A algorithm. Data were corrected for absorption effects using the multiscan method (SADABS). The structure was solved and refined using the Bruker SHELXTL software package.

RESULTS AND DISCUSSION

Representative synthetic schemes for preparing homoleptic (zDIP1−zDIP4) and heteroleptic (zDIP2′, zDIP3′) complexes are presented in Scheme 1. Mesityl substituents on the meso-position of the dipyrrin ligand were chosen to eliminate aryl rotation as a potential nonradiative deactivation pathway.[47] Dipyrrins DIP1−DIP4 were prepared from the corresponding pyrrole and mesitylaldehyde and used directly in consecutive reactions with DDQ and $Zn(OAc)_2$ to form the homoleptic complexes zDIP1−zDIP4 in total yields of 8−13%. The heteroleptic complexes were prepared from a reaction Zn(β-diketonate)$_2$ and the corresponding dipyrrin. Of the three ancillary ligands examined, pentane-2,4-dione (acac), 1,1,1,5,5,5-hexafluoropentane-2,4-dione, and 2,2,6,6-tetramethyl-3,5-heptanedione (dpm), pure heteroleptic complexes were successfully isolated only using the dpm ligand. As seen for other heteroleptic Zn complexes,[43,56] zDIP2′ and zDIP3′ disproportionate to their respective homoleptic complexes (zDIP2 and zDIP3) in chloroform over the course of several hours, as observed by NMR measurements (see SI). However, zDIP2′ and zDIP3′ are stable in the solid state and can be sublimed under vacuum without disproportionation. Single crystal X-ray analysis and high-resolution mass spectroscopy confirmed formation of zDIP2′ and zDIP3′. It should be noted that freshly prepared zDIP2′ and zDIP3′ solutions were used for each step of subsequent photophysical characterization to minimize the effects of disproportionation.

Crystal and Electronic Structure. Single crystal X-ray analysis was performed on zDIP3, zDIP4, zDIP2′, and zDIP3′; structures of representative homoleptic (zDIP3) and heteroleptic complexes (zDIP3′) are shown in Figure 2. The structures of zDIP3 and zDIP4 are similar to those published for zDIP1 and zDIP2.[54] The Zn−N bond lengths in the complexes range from 1.95 to 1.99 Å, while the Zn−O bond lengths in zDIP2′ and zDIP3′ vary between 1.95 and 1.97 Å. The zinc center in all the complexes adopts a distorted tetrahedral configuration with the two ligands held nearly

dx.doi.org/10.1021/jp506855t | J. Phys. Chem. C 2014, 118, 21834−21845

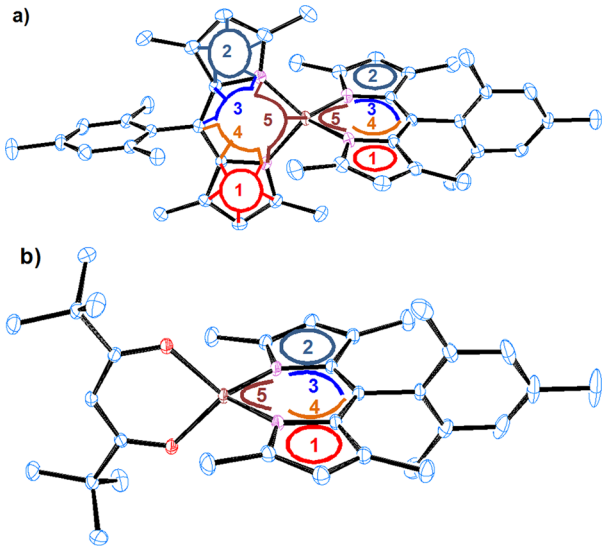

Figure 2. ORTEP diagrams of (a) zDIP3 and (b) zDIP3′ at 50% probability level. H atoms are omitted for clarity. Planes containing different groups of atoms are indicated by the colored lines.

perpendicular to each other. The dihedral angles between mean planes of the two dipyrrin ligands in zDIP1, zDIP2, zDIP3, and zDIP4 are 85.0°, 88.3°, 76.7°, and 83.4°, respectively, whereas values for the related angles between the two ligands of zDIP2′ and zDIP3′ are 87.8° and 89.8°, respectively. To evaluate the degree of distortion of the ligands, dihedral angles between the planes encompassing different groups of atoms as shown in Figure 2 were measured (Table 1). Compared to boron

Table 1. Dihedral Angles (deg) between Planes in Zinc Dipyrrins

planes	zDIP1[a]	zDIP2[a]	zDIP3	zDIP4	zDIP2′	zDIP3′
1,2	5.3	10.4	9.6	9.2	4.4	12.1
	3.1	8.5	6.5	8.8		
3,4	7.3	2.4	9.8	6.7	1.2	11.9
	3.9	2.1	3.3	2.8		
5,1	18.0	7.3	8.5	14.1	5.7	8.5
	5.9	4.5	7.4	6.3		
5,2	14.4	6.3	10.9	5.2	5.1	8.5
	2.9	4.4	3.5	7.3		
5,3	17.8	6.2	7.1	11.8	5.4	10.2
	6.1	1.7	6.0	5.3		
5,4	14.7	3.8	10.9	5.2	4.7	10.2
	4.3	1.7	4.5	7.3		
5,5	83.4	87.9	82.1	86.4	89.1	86.5

[a]From ref 54.

dipyrrin compounds, which are essentially flat,[57] the dipyrrin framework in the zinc dipyrrins is considerably more flexible, as dihedral angles between planes 1 and 2 vary from 3° to 18°. However, no clear correlation is apparent between the degree of alkylation and variation of the dihedral angles, indicating that the distortions are likely dictated by crystal packing forces.

In order to gain insight into the electronic structure of the zinc dipyrrin complexes, theoretical calculations were performed at the B3LYP/LACVP** level of theory. For simplicity, unsubstituted homoleptic zDIP and heteroleptic zDIP′ are presented, as it was found that they possess the same essential electronic features as their alkylated/arylated analogs. Structures of the optimized complexes, highest and next highest occupied molecular orbitals (HOMO, HOMO−1), and lowest and next lowest unoccupied molecular orbital (LUMO, LUMO +1), along with the corresponding energies, are shown in Figure 3. The HOMO (a_2 symmetry in the D_{2d} point group)

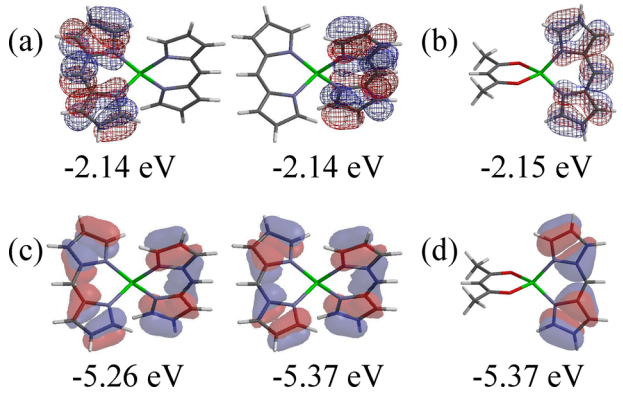

Figure 3. Frontier Kohn−Sham LUMOs (mesh) and energies for (a) zDIP and (b) zDIP′ and HOMOs (transparent) for (c) zDIP and (d) zDIP′. zDIP has D_{2d} symmetry and zDIP′ has C_{2v} symmetry.

and HOMO−1 (b_1) of zDIP localize on both dipyrrin ligands, while the doubly degenerate LUMOs are localized on separate dipyrrin ligands (Figure 3). Frontier orbitals of zDIP′ solely populate the dipyrrin ligand, excluding any participation of the β-diketonate ligand. Consistent with MO analysis, the calculated HOMO and LUMO energies of the two complexes are similar. There is little-to-no contribution from atomic orbitals on zinc to the frontier orbitals in either complex. The minor difference in energy between the HOMO and HOMO−1 in zDIP (0.11 eV) is indicative of very poor electronic coupling between the two orthogonal dipyrrin ligands in the ground state. The transition dipole moment of the metallodipyrrin fragment lies in the plane of the dipyrrin ligand, along the long axis of the ligand.[58] This places the transition dipole moments of the two dipyrrins in zDIPs orthogonal to each other, suggesting that there should be little or no excitonic or electronic coupling between the two dipyrrin ligands.

Photophysical Properties. The zinc dipyrrin complexes absorb strongly from 400 to 550 nm [ε = (1.01−1.17) × 10^5 M^{-1} cm^{-1}]. Representative absorption spectra of zDIP2 and zDIP2′ in different solvents are presented in Figure 4, and the emission spectra in the same solvents are given for zDIP2 in Figure 5. The photophysical properties of zDIP1−zDIP4 and zDIP2′ and zDIP3′ at room temperature are summarized in Table 2 and the SI. The absorption spectra and the principal band in the emission spectra are nearly independent of solvent polarity, indicating little change in the dipole moment or polarizability upon excitation.[59]

In cyclohexane, all of the complexes display emission spectra with small Stokes shifts indicative of a localized excited state. Representative spectra for zDIP2 and zDIP2′ are shown in Figure 6. The luminescent quantum yields (Φ_F) range between 0.08 and 0.66 and the fluorescence decays are single exponential with lifetimes (τ) that vary from 0.8 to 4.8 ns. The differences in Φ_F are due to significant variations in the rate constant for nonradiative decay (k_{nr}), as the rate constants for radiative decay (k_r) are similar among all the derivatives. The data reveals an interesting effect of alkylation on k_{nr}: zDIP2 ∼ zDIP1 < zDIP4 ∼ zDIP3 (Table 2). A similar effect of

dx.doi.org/10.1021/jp506855t | J. Phys. Chem. C 2014, 118, 21834−21845

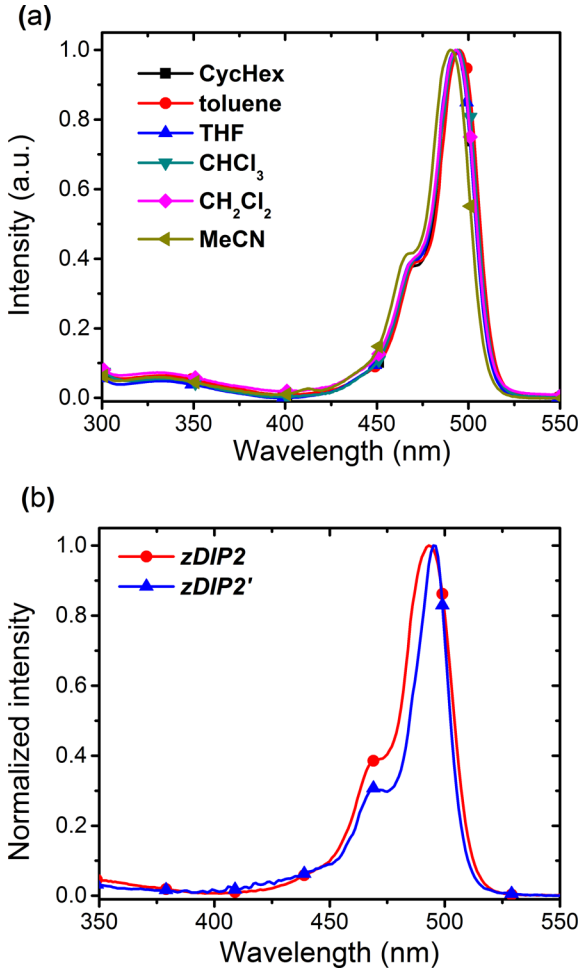

Figure 4. Absorption spectra of (a) zDIP2 in different solvents and (b) zDIP2 and zDIP2′ in cyclohexane.

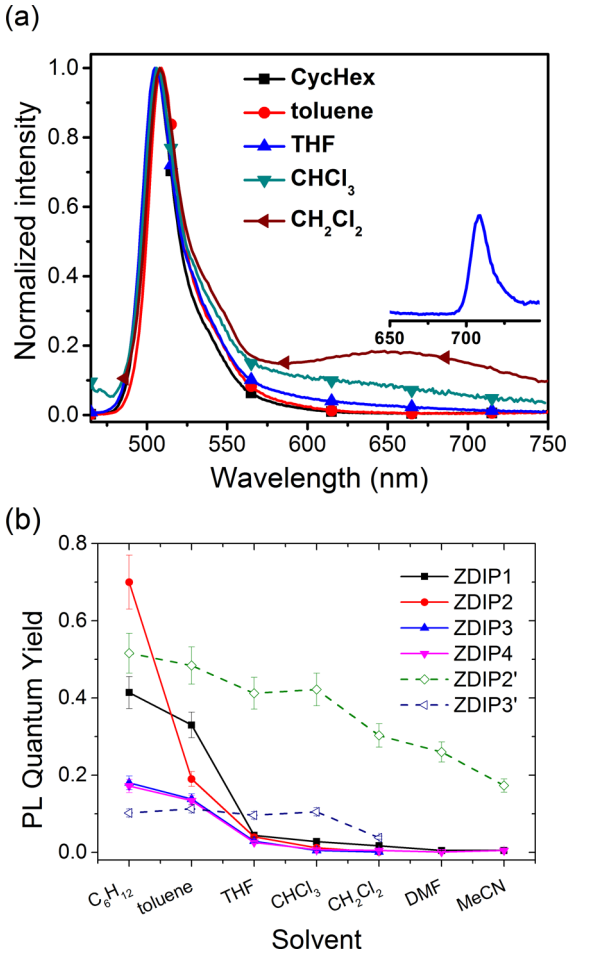

Figure 5. (a) Emission spectra of zDIP2 in various solvents (inset is the phosphorescence spectrum in 2-MeTHF at 77 K). (b) Quantum yield of zDIP1−zDIP4 and zDIP2′ and zDIP3′ plotted vs solvent from nonpolar to most polar.

alkylation on k_{nr} occurs in the heteroleptic complexes: zDIP2′ < zDIP3′. Comparing zDIP1 and zDIP2 shows that methylation at the α-position of the dipyrrin only slightly decreases k_{nr}, suggesting that hindering excited state distortion toward a planar coordination geometry has little effect on nonradiative decay. A more significant nonradiative decay process is evident for zDIP3 and zDIP4. Methyl substitution at the β-position, adjacent to the mesitylene substituted meso-carbon, leads to a marked enhancement in the observed k_{nr} values for these complexes. The effect is also seen when comparing zDIP2′ to zDIP3′, where β-methylation leads to a 6-fold increase in k_{nr}. The variation in k_{nr} for zDIP1−zDIP4 is roughly correlated with the fwhm of emission spectra (Figure 6, inset). The association of broader emission profiles with a faster k_{nr} suggests that structural distortion of the excited states increases internal conversion to the ground state. While one would have expected that libration of the mesityl group is more favorable in zDIP1 and zDIP2, thus increasing k_{nr} relative to their more sterically constrained analogs, zDIP3 and zDIP4, the opposite is true. A likely explanation for this is that steric interactions between the ortho-methyls on the mesityl group and the β-methyls of the dipyrrin exacerbate out-of-plane distortions on the dipyrrin ligand in zDIP3 and zDIP4, which is not expected to be the case for zDIP1 and zDIP2. Distortion of the dipyrrin from planarity will give both an increase in fwhm and k_{nr}, as observed here.[60]

While the absorption spectra for all the complexes are solvent-independent, the emission spectra of the homoleptic and heteroleptic derivatives exhibit distinct differences with respect to solvent polarity.[61] Representative emission spectra of zDIP2 measured in different solvents are shown in Figure 5a, data for luminescent quantum yields from zDIP1−zDIP4 and zDIP2′ and zDIP3′ are presented in Figure 5b, and other photophysical data are given in Table 2 and the SI. With increasing solvent polarity there is little change in the emission maxima; however, the quantum yields for zDIP1−zDIP4 sharply decrease and the excited state transients display multiexponential lifetimes with an increasing amplitude for a subnanosecond component. The subnanosecond component is faster than our instrument's response time (<22 ps). The multiexponential decay indicates that with increasing solvent polarity the majority of the S_1 population is going to a second state and only partially relaxing to the ground state by the radiative process (Figure S23 and Table S14, SI). For the least polar solvent, cyclohexane, single exponential decay is observed with lifetimes of 3.7, 4.8, and 1.4 ns for zDIP1, zDIP2, and zDIP3, respectively. The radiative rate constants for emission in cyclohexane fall in a narrow range of 0.11−0.14 ns^{-1}. In strong contrast, the luminescent quantum yields for zDIP2′ and zDIP3′ decline modestly in polar solvents and have radiative rate constants similar to those observed for zDIP1−zDIP3 in

dx.doi.org/10.1021/jp506855t | J. Phys. Chem. C 2014, 118, 21834−21845

Table 2. Photophysical Properties of Homoleptic and Heteroleptic Zinc Dipyrrin Complexes in Different Solvents at Room Temperature

	solvents	λ_{abs} (max/nm)	fwhm$_{ab}$ (cm^{-1})	λ_{em} (max/nm)	fwhm$_{em}$ (cm^{-1})	$\Delta\nu_{ab\text{-}em}$ (cm^{-1})	Φ_{PL}*
zDIP1	CycHex	484	1530	501	1260	638	0.47
	toluene	486	1443	503	1256	659	0.33
	THF	484	1437	494	1231	406	0.027
	CH_2Cl_2	485	1471	495	1131	429	0.017
	MeCN	481	1423	490	1180	396	<0.01
zDIP2	CycHex	493	983	506	944	501	0.66
	toluene	495	1022	509	959	567	0.19
	THF	493	1016	507	1013	586	0.09
	$CHCl_3$	494	1083	509	1013	592	0.05
	CH_2Cl_2	493	1074	508 (650)	1108	706	<0.01
	MeCN	490	1056	508	1494	736	
zDIP3	CycHex	489	1036	507	1500	676	0.16
	toluene	491	1120	510	1553	759	0.15
	THF	489	1092	511	1576	902	0.02
	CH_2Cl_2	488	1127	509 (653)	1591	819	<0.01
zDIP4	CycHex	506	1393	533	1480	1026	0.17
	toluene	508	1310	534	1593	958	0.15
	THF	505	1432	532	1604	982	0.026
	CH_2Cl_2	506	1403	528 (674)	1503	831	<0.01
zDIP2′	CycHex	495	733	503	863	305	0.52
	toluene	497	739	506	861	350	0.48
	THF	495	675	504	849	337	0.41
	$CHCl_3$	496	714	505	866	343	0.42
	CH_2Cl_2	495	777	505	885	388	0.30
	DMF	495	781	505	882	386	0.26
	MeCN	492	713	501	885	367	0.17
zDIP3′	CycHex	491	757	503	1311	467	0.085
	toluene	493	739	504	1240	463	0.085
	THF	490	723	503	1290	516	0.049
	$CHCl_3$	491	755	503	1220	485	0.050
	CH_2Cl_2	490	869	502	1290	485	0.037

*Photoluminescent quantum yield (±10%).

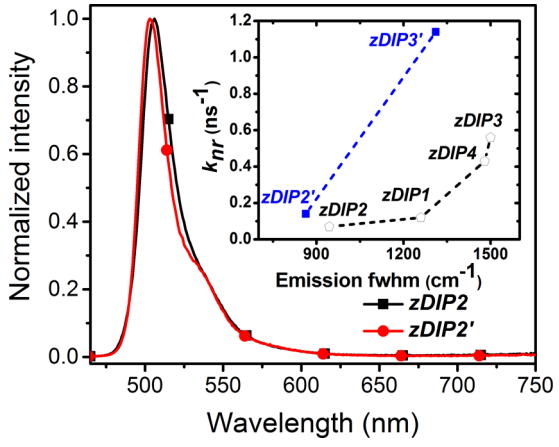

Figure 6. Emission spectra for zDIP2 and zDIP2′ in cyclohexane. (Inset) Full width at half-maximum (fwhm) of emission plotted vs nonradiative rate constant k_{nr} for zDIP1−zDIP4 and zDIP2′ and zDIP3′.

cyclohexane (i.e., for zDIP2′ k_{rad} = 0.15−0.19 ns^{-1} and for zDIP3′ k_{rad} = 0.11). For the mixed ligand complexes, we believe that the decrease in PL efficiency in polar solvents is due to their photoinstability. Both zDIP2′ and zDIP3′ disproportionate to Zn(acac)$_2$ and Zn(dipyrrin) thermally; the process is likely driven optically and accelerated in polar media. The pronounced decrease in PL efficiency for zDIP1−zDIP4 indicates that the locally excited state in the homoleptic derivatives equilibrates and deactivates to a weakly or nonemissive state in polar solvents. Moreover, a broad emission band emerges at low energy for zDIP2−zDIP4 in polar solvents (Figure 5a and SI). The emission band red-shifts and becomes more pronounced with increased solvent polarity. The luminescence quantum yield and emission lifetime data (Φ_F < 0.001, τ = 2.2 ns) indicate a very small radiative rate constant for this transition. However, the emission band is distinctly different from the phosphorescence of zDIP2 recorded at 77 K in 2-methyltetrahydofuran (2-MeTHF) (Figure 5a, inset). To determine if the broad emission at 650 nm originates from an excimer or aggregate, emission intensities of zDIP2 at 508 and 650 nm were measured at a range of concentrations (see the SI). The intensities of the two bands vary linearly with concentration, suggesting that excimer or aggregate emission is not responsible for the weak red emission in these compounds. Thus, the low-energy emission band is assigned to a charge transfer transition similar to that reported for meso-coupled boron dipyrrin compounds.[35] It is interesting to note that, in contrast to zDIP2−zDIP4, no low-energy emission is detected from nonalkylated zDIP1 in polar solvent (see the SI). Likewise, no comparable emission feature is observed in zDIP2′ or zDIP3′ in the same solvents.

dx.doi.org/10.1021/jp506855t | J. Phys. Chem. C 2014, 118, 21834−21845

The sharp decrease in luminescent efficiency from zDIP1−zDIP4 in polar solvents, along with the simultaneous appearance of an additional broad peak at longer wavelengths in the emission spectra of zDIP2−zDIP4, suggests a deactivation pathway to a weakly emissive state. This state most likely has CT character and is formed via a symmetry-breaking mechanism similar to that which occurs in other bichromophoric systems.[23,33,62−64] Further support for the hypothesis that the observed photophysical properties of zDIP1−zDIP4 are associated with SBCT is the weaker dependence on solvent polarity for the heteroleptic complexes zDIP2′ and zDIP3′, where SBCT is impossible.

Electrochemistry. Cyclic voltammetry (CV) and differential pulse voltammetry (DPV) for zDIP1−zDIP4 were carried out in dry THF under N_2, and the results are presented in Table 3. All of the complexes exhibit two distinct reversible

Table 3. Electrochemical and Optical Properties of Homoleptic Complexes[a]

	$E^{1/2}_{red\ 2}$ (V)	$E^{1/2}_{red\ 1}$ (V)	E_{OX} (V)	ΔE_{redox} (V)	ΔE_{00} (eV)	E_T (eV)	$\Delta E_{00} - \Delta E_{redox}$ (eV)
zDIP1	−2.33	−1.93	0.80	2.73	2.54	1.82	0.19
zDIP2	−2.42	−2.11	0.60	2.71	2.48	1.75	0.23
zDIP3	−2.79	−2.35	0.38	2.73	2.49	1.74	0.24
zDIP4	−2.82	−2.44	0.24	2.68	2.40	1.72	0.28
			0.37				

[a]Electrochemical values (±0.02 V) were determined by differential pulsed voltammetry (DPV) vs Fc^+/Fc. The optical gap E_{00} is defined by the midpoint between absorption and emission spectra in THF. Triplet energies were measured in 2-methyltetrahydrofuran at 77 K.

reduction peaks and one irreversible oxidation peak, with the exception of zDIP4, where two quasireversible oxidation peaks are observed. The redox potentials are cathodically shifted by around 200 mV upon addition of two alkyl groups per ligand; however, the difference between the first oxidation and reduction potentials (electrochemical gap, ΔE_{redox}) remains relatively constant for all the derivatives. This data can be used to evaluate the thermodynamic requirements for zDIP1−zDIP4 to undergo photoinduced SBCT. Stabilization of the CT state in zDIP1−zDIP4 is required to enable SBCT, since ΔE_{redox} is greater than the optical S_1 gap (ΔE_{00}). The required stabilization energies vary from 0.19 to 0.28 eV (see Table 3).[8,27] Thus, while nonpolar solvents disfavor SBCT, polar solvents such as dichloromethane (ε_s = 8.9) or acetonitrile (ε_s = 37.5) provide a stabilization energy estimated to exceed 0.3 eV[8,27] and can therefore promote SBCT.

Spectroelectrochemical measurements were also performed in order to identify absorption transitions characteristic of the CT state. The absorption profile for the one-electron-reduced form of zDIP1 is broader than the neutral complex and has enhanced transitions between 370 and 430 nm along with a distinct peak at 517 nm (Figure 7). Unfortunately, the irreversible nature of electrochemical oxidation in zDIP1−zDIP3 precluded optical characterization of the cation. Likewise, the low stability of the zDIP4 cation prevented characterization using spectroelectrochemical methods.

Transient Absorption Spectroscopy. Femtosecond and nano-to-microsecond transient absorption (TA) measurements were performed to confirm the presence of SBCT and to study the kinetics of such processes. Femtosecond TA values of zDIP1 in cyclohexane, toluene, dichloromethane, and acetonitrile are presented in Figure 8. Other femtosecond TA spectra of zDIP2 and zDIP3 in cyclohexane, toluene, and acetonitrile are shown in the SI. In cyclohexane (Figure 8a), excitation at 500 nm populates the S_1 state, as observed by a ground-state bleach from 430 to 500 nm (compare to Figure 4), stimulated emission (520−600 nm, compare Figure 6), and excited state absorption at 345 nm. The stimulated emission remains over the probing time (1.1 ns), resulting in a minimal shift of the bleach peak (Figure 8a).

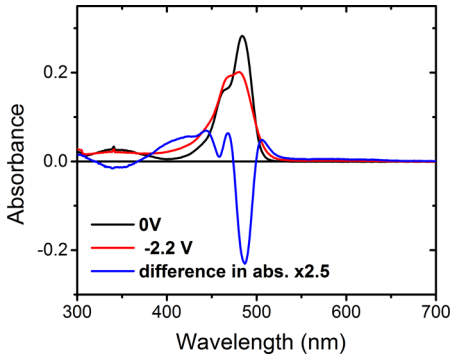

Figure 7. Spectroelectrochemical data of zDIP1 in dichloromethane under negative applied bias.

In polar solvents such as dichloromethane (Figure 8c) and acetonitrile (Figure 8d), stimulated emission and excited state absorption at 345 nm from S_1 appear immediately following excitation, similar to what is observed in cyclohexane. However, over the course of 4−6 ps, the stimulated emission band disappears and new induced absorption bands at 370 and 517 nm grow in. In contrast to the TA spectrum in cyclohexane, the disappearance of the stimulated emission results in the shift of the bleach peak (Figure 8c,d). The induced absorption at 517 nm is similar to that of the zDIP1 anion [see Figures 7 and S25 (SI) for a detailed comparison]. Since the induced absorption peak at 370 evolves with similar kinetics to that at 517 nm, we assign the 370 nm peak to the new excited state as well. This state is assigned as the SBCT species; note that the absence of characteristic SBCT absorptions in cyclohexane indicates that stabilization by polar solvents is required to favor SBCT over the local excited state, in agreement with the electrochemical analysis. The increase in the ground-state bleach during the first 10 ps (Figure 8c,d) is a direct consequence of SBCT. This is because only one of the DIP ligands in the complex is bleached upon initial photoexcitation, whereas the second ligand is subsequently bleached upon SBCT; thus, the bleach increases approximately by a factor of 2.

In a weakly polar solvent, toluene (Figure 8b), both S_1 stimulated emission and induced absorption at 370 nm are observed over the probing time of 1.1 ns, suggesting that the kinetic evolution of the transients is different from what was observed in either polar solvents or cyclohexane. The induced absorption at 370 nm indicates SBCT of zDIP1 in toluene; however, the induced absorption at 517 nm is hidden due to the overlap with the stimulated emission band. Additionally, the stimulated emission persists over the probing time (1.1 ns), which is much longer than that in acetonitrile or dichloromethane. The luminescent efficiency of zDIP1 in toluene is also much higher than that in acetonitrile and dichloromethane (Table 2). Similar results were seen for zDIP2 and zDIP3 in toluene (SI). These observations can be explained by the presence of an equilibrium between the local excited state S_1

dx.doi.org/10.1021/jp506855t | J. Phys. Chem. C 2014, 118, 21834−21845

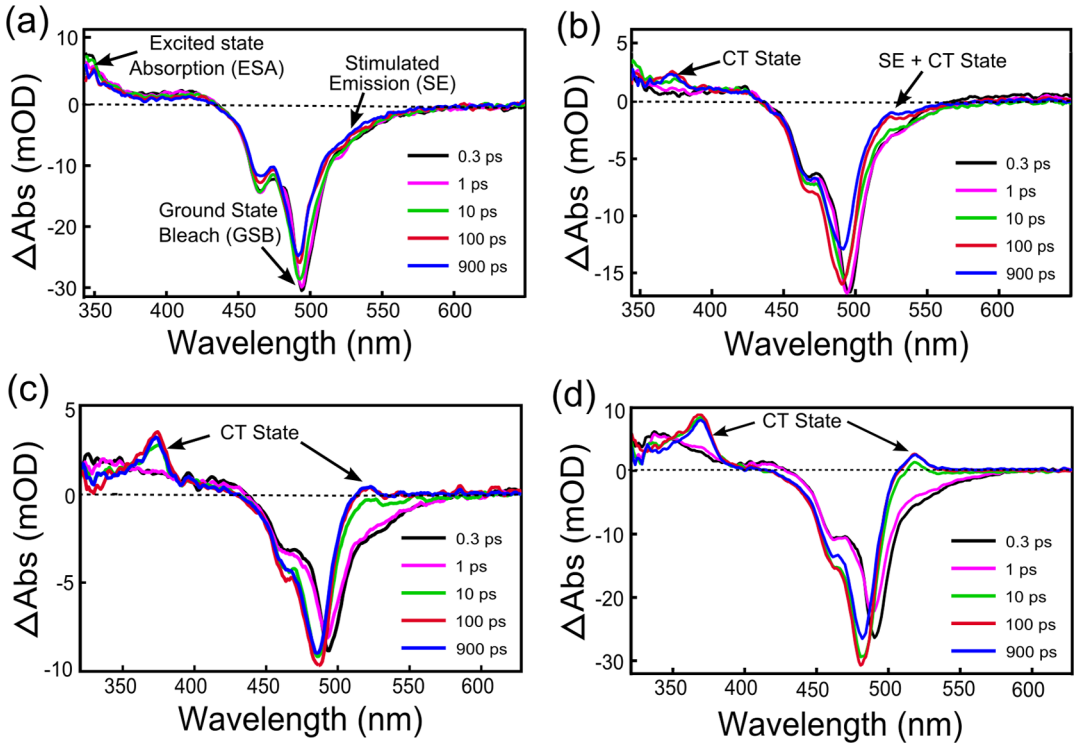

Figure 8. Femtosecond transient absorption of zDIP1 in (a) cyclohexane, (b) toluene, (c) dichloromethane, and (d) acetonitrile. Excitation at 500 nm and pump fluence of 160 $\mu J/cm^2$ were used for all, except panel c, which was performed at 70 $\mu J/cm^2$.

and CT states in toluene. We propose that solvation by weakly polar toluene lowers the energy of the CT state close to that of the locally excited state. A similar equilibrium between locally excited and CT states of 9,9′-bianthryl was reported in weakly polar media.[26,29,30] In more polar solvents, large solvation energies further stabilize the CT states, shifting the equilibrium to formation of the charge transfer species.

On the basis of the femtosecond TA measurements, a simplified Jablonski diagram is proposed to explain the obtained results (Figure 9). Global fitting of TA data from

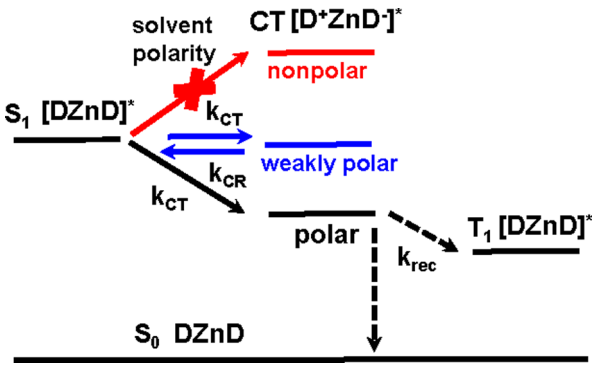

Figure 9. A simplified Jablonski diagram illustrating the dependence of the symmetry-breaking charge transfer process on solvent polarity. k_{rec} is the total rate for recombination to either the triplet or ground state.

zDIP1−zDIP3 in different solvents has been performed using the proposed scheme, and the results are presented in Table 4 (A detailed description of the fitting scheme and the species-associated spectra are shown in the SI). SBCT does not occur in nonpolar cyclohexane, and the kinetics of transient species was fitted to a monoexponential decay with the lifetimes of 4.5, 4.8, and 1.4 ns for zDIP1, zDIP2, and zDIP3, respectively. These decay times are in good agreement with fluorescence lifetimes of the respective compounds in cyclohexane (Table S14, SI).

Table 4. Kinetic Rates for Different Processes of zDIP1−zDIP3 in Different Solvents Determined by Femtosecond Transient Absorption Measurements

	solvent	$1/k_{CT}$ (ps)	$1/k_{CR}$ (ps)	$1/k_{rec}$ (ns)	$1/(k_r+k_{nr})$ (ns)
zDIP1	CycHex				4.5 ± 0.1
	toluene	14 ± 1	22 ± 2	3.5 ± 0.2	3.0 ± 0.3
	CH_2Cl_2	5.5 ± 0.5		3.3 ± 0.3	
	MeCN	3.6 ± 0.5		2.1 ± 0.2	
zDIP2	CycHex				4.8 ± 0.3
	toluene	8.6 ± 2	15.5 ± 2	4.0 ± 0.5	3.9 ± 0.3
	MeCN	1.1 ± 0.3		0.9 ± 0.1	
zDIP3	CycHex				1.4 ± 0.3
	toluene	2.3 ± 1	11.2 ± 3	2.5 ± 0.3	2.1 ± 0.2
	MeCN	1.0 ± 0.5		1.4 ± 0.1	

TA data of zDIP1 in toluene were fitted with a different model to account for an equilibrium between the local excited state S_1 and the CT state. The forward and backward rates ($1/k_{CT}$ and $1/k_{CR}$) between the S_1 and the CT states are 13 and 25 ps, respectively. Since these rates are 2 orders of magnitude faster than both the charge recombination rate of the CT state ($1/k_{rec}$ = 3.5 ns) and the decay rate of the local excited state (τ = 3.0 ns), our assumption about a fast equilibrium is indeed reasonable.

In polar dichloromethane, the fitting yields rates of 5.5 ps and 3.3 ns for the formation ($1/k_{CT}$) and the recombination ($1/k_{rec}$) of the CT state of zDIP1, respectively. In acetonitrile, the rates for formation and recombination of the CT state are faster compared to those in dichloromethane ($1/k_{CT}$ = 3.6 ps

dx.doi.org/10.1021/jp506855t | J. Phys. Chem. C 2014, 118, 21834−21845

and $1/k_{rec}$ = 2.1 ns). Generally, the rate for formation of the CT state in polar solvents ($1/k_{CT}$ = 1.1−5.5 ps) is 3 orders of magnitude faster than that for recombination ($1/k_{rec}$ = 0.9−3.3 ns) (Table 4).

Interestingly, the femtosecond TA measurements of zDIP2 and zDIP3 in acetonitrile (Figure 10 and the SI) show faster

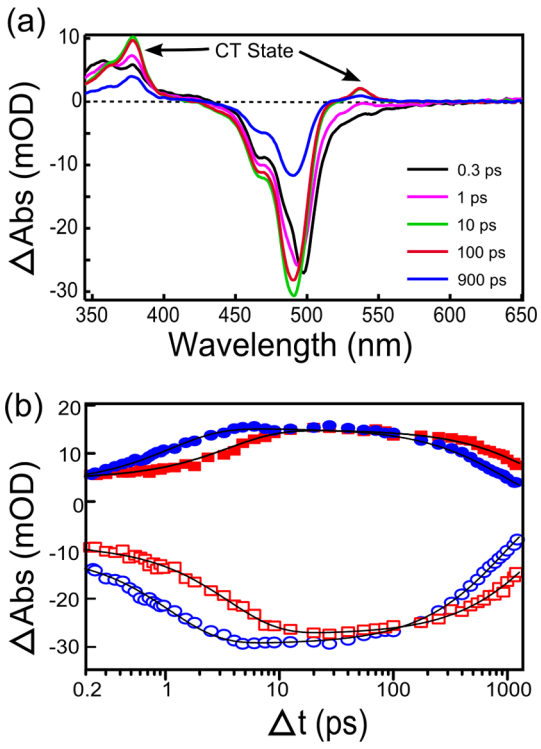

Figure 10. (a) Femtosecond transient absorption of zDIP2 with 500 nm excitation in acetonitrile. (b) Comparison of dynamics for formation of the CT state (monitored at 370 nm, ×2) (filled) and ground state bleach (open) between zDIP1 (red squares) and zDIP2 (blue circles) in acetonitrile.

rates for both formation and recombination of the CT state ($1/k_{CT}$ = 1.1, 1.0 ps and $1/k_{rec}$ = 0.9, 1.4 ns for zDIP2 and zDIP3, respectively) compared to zDIP1. The two dipyrrin ligands of zDIP2 and zDIP3 are expected to have less torsional freedom around the Zn center relative to zDIP1 due to the presence of methyl groups at the α-positions. This steric hindrance constrains the ligands to adopt a more orthogonal configuration. Without these steric impediments, the ligands can twist in the excited state, promoting interligand $\pi-\pi$ interactions. This $\pi-\pi$ interaction will lower the energy of the excited state, making the S_1 state less energetically favorable for forming the SBCT state.

While femtosecond TA measurements of zDIP1−zDIP3 show that SBCT occurs in weakly polar to polar solvents, questions about deactivation pathways of the CT state still remain open. Schutz and Schmidt reported that the CT state of 9,9′-bianthryl recombined radiatively to the ground state or nonradiatively to triplet states in polar solvents; the nonradiative CT → S_0 internal conversion was negligible.[26] In contrast to 9,9′-bianthryl, poor electronic coupling makes the CT state in zDIP1−zDIP4 at best only weakly emissive, indicating nonradiative deactivation via either direct CT → S_0 internal conversion or CT → T_1 recombination. Direct internal conversion does occur as femtosecond TA measurements show partial recovery of the ground state bleach with a concomitant decrease of the CT induced absorption (Figure 10b). On the other hand, energies for the triplet states of zDIP2−zDIP4 measured at 77 K in 2-MeTHF (1.75, 1.74, and 1.72 eV, respectively, see Table 3) are lower than those for the CT states (1.92, 1.90, and 1.84 eV, respectively, as estimated from maxima of the CT emission peaks in dichloromethane). Even higher energies for the CT states are expected in less polar solvents. Thus, CT → T_1 charge recombination is also thermodynamically favorable.

Deactivation of the CT states was further probed by performing nano-to-microsecond transient absorption measurements on zDIP1 in different solvents; results are presented in Figure 11 and the SI. In all solvents, induced absorption peaks from the CT state are absent within the instrument response time (approximately 20 ns), and new induced absorption bands appear at 350−450 nm (λ_{max} = 420 nm) and 550−600 nm. To elucidate the origin of these new induced absorption features, femtosecond TA of zDIP1 was measured in dichloromethane/methyl iodide (CH_2Cl_2/CH_3I 1/4) (Figure 11c), a solvent

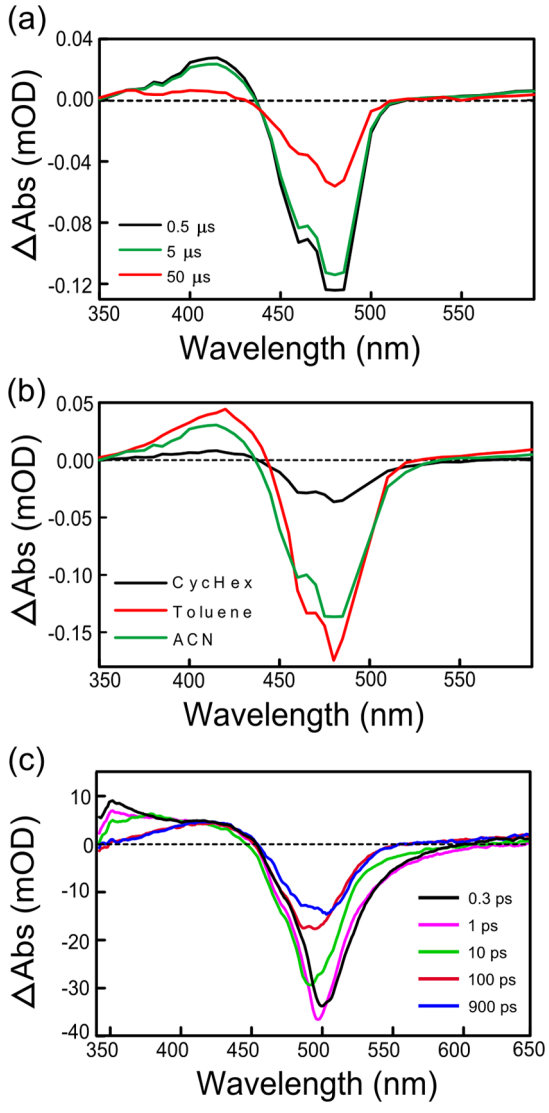

Figure 11. Nano-to-millisecond transient absorption of zDIP1 in (a) acetonitrile and (b) different solvents at 0.5 μs and (c) femtosecond transient absorption of zDIP1 in CH_2Cl_2/CH_3I (1/4).

dx.doi.org/10.1021/jp506855t | J. Phys. Chem. C 2014, 118, 21834−21845

mixture that is expected to accelerate intersystem crossing from the excited singlet state to the triplet state.[65] The induced absorption in this mixture matches well with the microsecond TA spectrum of zDIP1 in acetonitrile (Figure 11a). Thus, the induced absorption features from 20 ns to milliseconds observed in acetonitrile are assigned exclusively to the triplet state. Similar results were obtained in toluene. Formation of the triplet state in cyclohexane was also observed; however, the signal intensity is much weaker than that observed in more polar solvents (Figure 11b). We speculate that formation of the triplet state via $S_1 \rightarrow T_1$ intersystem crossing is less efficient in cyclohexane than via $S_1 \rightarrow CT \rightarrow T_1$ recombination, as observed in toluene and acetonitrile. By fitting the microsecond TA traces to a single exponential decay, triplet lifetimes ($1/k_{T1}$) for zDIP1 were determined to be 16, 50, and 33 μs in cyclohexane, toluene, and acetonitrile, respectively.

CONCLUSION

Homoleptic zinc dipyrrins zDIP1−zDIP4 exhibit photophysical properties that are strongly influenced by solvent polarity. These solvent-dependent properties are shown to occur by deactivation of the locally excited state via a symmetry-breaking charge transfer process. Transient absorption measurements revealed that SBCT proceeds in polar solvents at a rate 2 orders of magnitude faster than charge recombination. This fast charge transfer rate (1.0−14 ps), in combination with slower charge recombination rate (1.0−3.5 ns), is a desirable property for materials used in OPVs, as it allows sufficient time for charge separation at a donor/acceptor interface.

The weakly emissive nature of the CT state of zinc dipyrrins is in contrast to the efficient CT emission observed for bianthryl[23,26,66] and biperylenyl.[31] In the latter complexes, significant electronic coupling exists between the two chromophoric units. For zDIP1−zDIP4, poor molecular orbital overlap and weak dipolar coupling between the two nearly orthogonal dipyrrin ligands, as seen in the computational studies and crystal structure (Figures 2 and 3), can be used to explain the decreased emissivity. It is interesting to note that no low energy emission was detected from nonalkylated zinc dipyrrin zDIP1 in polar solvent in contrast to zDIP2−zDIP4 (see the SI).

The SBCT also sheds light on the origin of the low luminescent efficiencies exhibited by homoleptic zinc dipyrrin complexes in polar and weakly polar solvents, especially when compared to their heteroleptic counterparts. Our results suggest that metal complexes containing a single dipyrrin ligand are promising candidates as highly fluorescent probes in a range of applications; however, the instability to disproportionation is a drawback for the Zn derivatives.

Finally, this study demonstrates that SBCT can occur in systems where the chromophores remain weakly coupled in the excited state. It is interesting to note that other molecules that have been shown to undergo SBCT exhibit some degree of electronic overlap between chromophoric units, as indicated using calculated frontier orbitals.[35,66] Additionally, the previous systems have a degree of rotational freedom around a σ-bond, leading to a twisted internal charge transfer mechanism,[27] whereas the zDIP1−zDIP4 complexes are capable of SBCT, even when rotational motion is severely restricted between the orthogonal ligands. Similarly, weak intermolecular couplings are ubiquitous in the neat solid, where the dielectric constant should be comparable to that of toluene (ε_s = 2.4). Thus, formation of CT states should be a relatively common occurrence upon photoexcitation of related chromophores in the solid state.

ASSOCIATED CONTENT

Supporting Information

^{1}H and ^{13}C NMR spectra of zDIP3, zDIP4, zDIP2′, and zDIP3′; absorption and emission spectra of zDIP1−zDIP4 and zDIP2′ and zDIP3′ in various solvents and emission spectra at 77 K in 2-MeTHF; CV and DPV traces for zDIP1−zDIP4 in THF and for zDIP1 in CH_2Cl_2; femtosecond TA spectra of zDIP2 and zDIP3 in cyclohexane and toluene and of zDIP3 in acetonitrile along with the global analysis; microsecond TA spectra of zDIP1 in cyclohexane and toluene; solvent polarity dependent time-resolved photoluminescence of zDIP1−zDIP3; perspective views for X-ray structures of zDIP4 and zDIP2′; electron density surfaces calculated for zDIP1 and zDIP2; tables of X-ray data collection details, sample and crystal data, data collection, and structure refinement for zDIP3, zDIP4, zDIP2′, and zDIP3′; and X-ray structure files for compounds zDIP3, zDIP4, zDIP2′, and zDIP3′ in CIF format. This material is available free of charge via the Internet at http://pubs.acs.org.

AUTHOR INFORMATION

Corresponding Author

*E-mail: met@usc.edu.

Notes

The authors declare the following competing financial interest(s): One of the authors, Mark Thompson, has a financial interest in Nanoflex Power Corp., which one of the sponsors of this work.

ACKNOWLEDGMENTS

We thank Dr. Ralf Haiges for the help with crystallographic studies and Dr. Sean Roberts for helpful discussion regarding the TA data. We acknowledge financial support from following organizations: the synthesis and characterization of zinc dipyrrins were supported by the Nanoflex Power Corp.; X-ray crystallography was performed on a Bruker APEX II CCD system, acquired with funds provided by the NSF CRIF program (Award 1048807); some of the NMR spectra were recorded on a Varian 400-MR spectrometer, acquired with funds provided by the NSF CRIF program (Award 0840366); ns-to-ms TA experiments were performed at the Beckman Institute Laser Resource Center at Caltech; M.E.E. was supported by NIH Grant RO1-DK019038; ultrafast (fs-to-ns) TA studies were supported by the Center for Energy Nanoscience (CEN) at USC. CEN is an Energy Frontier Research Center funded by the U.S. Department of Energy, Office of Science, Office of Basic Energy Sciences (DE-SC0001013).

REFERENCES

(1) Huang, L.; Ponomarenko, N.; Wiederrecht, G. P.; Tiede, D. M. Cofactor-Specific Photochemical Function Resolved by Ultrafast Spectroscopy in Photosynthetic Reaction Center Crystals. *Proc. Natl. Acad. Sci. U. S. A.* **2012**, *109*, 4851−4856.

(2) Moore, L. J.; Zhou, H. L.; Boxer, S. G. Excited-State Electronic Asymmetry of the Special Pair in Photosynthetic Reaction Center Mutants: Absorption and Stark Spectroscopy. *Biochemistry* **1999**, *38*, 11949−11960.

(3) Mueller, M. G.; Slavov, C.; Luthra, R.; Redding, K. E.; Holzwarth, A. R. Independent Initiation of Primary Electron Transfer in the Two

Branches of the Photosystem I Reaction Center. *Proc. Natl. Acad. Sci. U. S. A.* **2010**, *107*, 4123−4128.
(4) Xiong, L.; Seibert, M.; Gusev, A. V.; Wasielewski, M. R.; Hemann, C.; Hille, C. R.; Sayre, R. T. Substitution of a Chlorophyll into the Inactive Branch Pheophytin-Binding Site Impairs Charge Separation in Photosystem II. *J. Phys. Chem. B* **2004**, *108*, 16904−16911.
(5) Lathrop, E. J. P.; Friesner, R. A. Simulation of Optical Spectra from the Reaction Center of *Rb. sphaeroides*. Effects of an Internal Charge-Separated State of the Special Pair. *J. Phys. Chem.* **1994**, *98*, 3056−3066.
(6) Lockhart, D. J.; Boxer, S. G. Magnitude and Direction of the Change in Dipole Moment Associated with Excitation of the Primary Electron Donor in *Rhodopseudomonas sphaeroides* Reaction Centers. *Biochemistry* **1987**, *26*, 664−668.
(7) Meech, S. R.; Hoff, A. J.; Wiersma, D. A. Evidence for a Very Early Intermediate in Bacterial Photosynthesis. A Photon-Echo and Hole-Burning Study of the Primary Donor Band in *Rhodopseudomonas sphaeroides*. *Chem. Phys. Lett.* **1985**, *121*, 287−292.
(8) Vauthey, E. Photoinduced Symmetry-Breaking Charge Separation. *ChemPhysChem* **2012**, *13*, 2001−2011.
(9) Barber, J.; Tran, P. D. From Natural to Artificial Photosynthesis. *J. R. Soc., Interface* **2013**, *10*, 20120984.
(10) Bottari, G.; Trukhina, O.; Ince, M.; Torres, T. Towards Artificial Photosynthesis: Supramolecular, Donor−Acceptor, Porphyrin- and Phthalocyanine/Carbon Nanostructure Ensembles. *Coord. Chem. Rev.* **2012**, *256*, 2453−2477.
(11) Cowan, A. J.; Durrant, J. R. Long-Lived Charge Separated States in Nanostructured Semiconductor Photoelectrodes for the Production of Solar Fuels. *Chem. Soc. Rev.* **2013**, *42*, 2281−2293.
(12) Izumi, Y. Recent Advances in the Photocatalytic Conversion of Carbon Dioxide to Fuels with Water and/or Hydrogen Using Solar Energy and Beyond. *Coord. Chem. Rev.* **2013**, *257*, 171−186.
(13) Luo, S.-P.; Mejia, E.; Friedrich, A.; Pazidis, A.; Junge, H.; Surkus, A.-E.; Jackstell, R.; Denurra, S.; Gladiali, S.; Lochbrunner, S.; Beller, M. Photocatalytic Water Reduction with Copper-Based Photosensitizers: A Noble-Metal-Free System. *Angew. Chem., Int. Ed.* **2013**, *52*, 419−423.
(14) Manbeck, G. F.; Brewer, K. J. Photoinitiated Electron Collection in Polyazine Chromophores Coupled to Water Reduction Catalysts for Solar H_2 Production. *Coord. Chem. Rev.* **2013**, *257*, 1660−1675.
(15) Pillai, S.; Ravensbergen, J.; Antoniuk-Pablant, A.; Sherman, B. D.; van Grondelle, R.; Frese, R. N.; Moore, T. A.; Gust, D.; Moore, A. L.; Kennis, J. T. M. Carotenoids as Electron or Excited-State Energy Donors in Artificial Photosynthesis: An Ultrafast Investigation of a Carotenoporphyrin and a Carotenofullerene Dyad. *Phys. Chem. Chem. Phys.* **2013**, *15*, 4775−4784.
(16) Woller, J. G.; Hannestad, J. K.; Albinsson, B. Self-Assembled Nanoscale DNA−Porphyrin Complex for Artificial Light Harvesting. *J. Am. Chem. Soc.* **2013**, *135*, 2759−2768.
(17) Young, K. J.; Martini, L. A.; Milot, R. L.; Snoeberger, R. C., III; Batista, V. S.; Schmuttenmaer, C. A.; Crabtree, R. H.; Brudvig, G. W. Light-Driven Water Oxidation for Solar Fuels. *Coord. Chem. Rev.* **2012**, *256*, 2503−2520.
(18) Banerji, N.; Fuerstenberg, A.; Bhosale, S.; Sisson, A. L.; Sakai, N.; Matile, S.; Vauthey, E. Ultrafast Photoinduced Charge Separation in Naphthalene Diimide Based Multichromophoric Systems in Liquid Solutions and in a Lipid Membrane. *J. Phys. Chem. B* **2008**, *112*, 8912−8922.
(19) Bhosale, S.; Sisson, A. L.; Talukdar, P.; Fuerstenberg, A.; Banerji, N.; Vauthey, E.; Bollot, G.; Mareda, J.; Roger, C.; Wuerthner, F.; Sakai, N.; Matile, S. Photoproduction of Proton Gradients with Pi-Stacked Fluorophore Scaffolds in Lipid Bilayers. *Science* **2006**, *313*, 84−86.
(20) Kishore, R. S. K.; Kel, O.; Banerji, N.; Emery, D.; Bollot, G.; Mareda, J.; Gomez-Casado, A.; Jonkheijm, P.; Huskens, J.; Maroni, P.; Borkovec, M.; Vauthey, E.; Sakai, N.; Matile, S. Ordered and Oriented Supramolecular N/P-Heterojunction Surface Architectures: Completion of the Primary Color Collection. *J. Am. Chem. Soc.* **2009**, *131*, 11106−11116.
(21) Sisson, A. L.; Sakai, N.; Banerji, N.; Fuerstenberg, A.; Vauthey, E.; Matile, S. Zipper Assembly of Vectorial Rigid-Rod Pi-Stack Architectures with Red and Blue Naphthalenediimides: Toward Supramolecular Cascade N/P-Heterojunctions. *Angew. Chem., Int. Ed.* **2008**, *47*, 3727−3729.
(22) Asami, N.; Takaya, T.; Yabumoto, S.; Shigeto, S.; Hamaguchi, H.-o.; Iwata, K. Two Different Charge Transfer States of Photoexcited 9,9′-Bianthryl in Polar and Nonpolar Solvents Characterized by Nanosecond Time-Resolved Near-IR Spectroscopy in the 4500−10 500 cm^{-1} Region. *J. Phys. Chem. A* **2010**, *114*, 6351−6355.
(23) Piet, J. J.; Schuddeboom, W.; Wegewijs, B. R.; Grozema, F. C.; Warman, J. M. Symmetry Breaking in the Relaxed S_1 Excited State of Bianthryl Derivatives in Weakly Polar Solvents. *J. Am. Chem. Soc.* **2001**, *123*, 5337−5347.
(24) Schneide, F.; Lippert, E. Electron Spectra and Electron Structure of 9,9′-Bianthryl. *Ber. Bunsen-Ges. Phys. Chem.* **1968**, *72*, 1155−1160.
(25) Schneide, F.; Lippert, E. Molecular Calculations for Pi-Electron Structure of 9,9′-Dianthryl. *Ber. Bunsen-Ges. Phys. Chem.* **1970**, *74*, 624−630.
(26) Schutz, M.; Schmidt, R. Deactivation of 9,9′-Bianthryl in Solution Studied by Photoacoustic Calorimetry and Fluorescence. *J. Phys. Chem.* **1996**, *100*, 2012−2018.
(27) Grabowski, Z. R.; Rotkiewicz, K.; Rettig, W. Structural Changes Accompanying Intramolecular Electron Transfer: Focus on Twisted Intramolecular Charge-Transfer States and Structures. *Chem. Rev.* **2003**, *103*, 3899−4031.
(28) Rettig, W.; Zander, M. Broken Symmetry in Excited-States of 9,9′-Bianthryl. *Ber. Bunsen-Ges.-Phys. Chem. Chem. Phys.* **1983**, *87*, 1143−1149.
(29) Zander, M.; Rettig, W. Fluorescence Studies on Solvent-Induced Intramolecular Charge Separation in Symmetric Biaryls. *Chem. Phys. Lett.* **1984**, *110*, 602−610.
(30) Fritz, R.; Rettig, W.; Nishiyama, K.; Okada, T.; Muller, U.; Mullen, K. Excitonic and Charge Transfer States in Oligomeric 9,10-Anthrylene Chains. *J. Phys. Chem. A* **1997**, *101*, 2796−2802.
(31) Dobkowski, J.; Grabowski, Z. R.; Paeplow, B.; Rettig, W.; Koch, K. H.; Mullen, K.; Lapouyade, R. Intramoleuclar Charge-Transfer States in Symmetrical Biaryls—The Unusual Case of Biperylenyl. *New J. Chem.* **1994**, *18*, 525−533.
(32) Giaimo, J. M.; Lockard, J. V.; Sinks, L. E.; Scott, A. M.; Wilson, T. M.; Wasielewski, M. R. Excited Singlet States of Covalently Bound, Cofacial Dimers and Trimers of Perylene-3,4:9,10-bis(dicarboximide)-s. *J. Phys. Chem. A* **2008**, *112*, 2322−2330.
(33) Khandelwal, H.; Mallia, A. R.; Cheriya, R. T.; Hariharan, M. Effect of Temperature on Symmetry Breaking Excited State Charge Separation: Restoration of Symmetry at Elevated Temperature. *Phys. Chem. Chem. Phys.* **2012**, *14*, 15282−15285.
(34) Markovic, V.; Villamaina, D.; Barabanov, I.; Daku, L. M. L.; Vauthey, E. Photoinduced Symmetry-Breaking Charge Separation: The Direction of the Charge Transfer. *Angew. Chem., Int. Ed.* **2011**, *50*, 7596−7598.
(35) Whited, M. T.; Patel, N. M.; Roberts, S. T.; Allen, K.; Djurovich, P. I.; Bradforth, S. E.; Thompson, M. E. Symmetry-Breaking Intramolecular Charge Transfer in the Excited State of Meso-Linked BODIPY Dyads. *Chem. Commun.* **2011**, *48*, 284−286.
(36) Loudet, A.; Burgess, K. BODIPY Dyes and Their Derivatives: Syntheses and Spectroscopic Properties. *Chem. Rev.* **2007**, *107*, 4891−4932.
(37) Wood, T. E.; Thompson, A. Advances in the Chemistry of Dipyrrins and Their Complexes. *Chem. Rev.* **2007**, *107*, 1831−1861.
(38) Clarke, T. M.; Durrant, J. R. Charge Photogeneration in Organic Solar Cells. *Chem. Rev.* **2010**, *110*, 6736−6767.
(39) Mbatia, H. W.; Burdette, S. C. Photochemical Tools for Studying Metal Ion Signaling and Homeostasis. *Biochemistry* **2012**, *51*, 7212−7224.
(40) Nolan, E. M.; Lippard, S. J. Small-Molecule Fluorescent Sensors for Investigating Zinc Metalloneurochemistry. *Acc. Chem. Res.* **2009**, *42*, 193−203.

(41) Crawford, S. M.; Ali, A. A.-S.; Cameron, T. S.; Thompson, A. Synthesis and Characterization of Fluorescent Pyrrolyldipyrrinato Sn(IV) Complexes. *Inorg. Chem.* **2011**, *50*, 8207−8213.
(42) Ding, Y.; Xie, Y.; Li, X.; Hill, J. P.; Zhang, W.; Zhu, W. Selective and Sensitive "Turn-on" Fluorescent Zn^{2+} Sensors Based on Di- and Tripyrrins with Readily Modulated Emission Wavelengths. *Chem. Commun.* **2011**, *47*, 5431−5433.
(43) Filatov, M. A.; Lebedev, A. Y.; Mukhin, S. N.; Vinogradov, S. A.; Cheprakov, A. V. Pi-Extended Dipyrrins Capable of Highly Fluorogenic Complexation with Metal Ions. *J. Am. Chem. Soc.* **2010**, *132*, 9552−9554.
(44) Kusaka, S.; Sakamoto, R.; Kitagawa, Y.; Okumura, M.; Nishihara, H. An Extremely Bright Heteroleptic Bis(dipyrrinato)zinc-(II) Complex. *Chem.-Asian J.* **2012**, *7*, 907−910.
(45) Sakamoto, N.; Ikeda, C.; Yamamura, M.; Nabeshima, T. Structural Interconversion and Regulation of Optical Properties of Stable Hypercoordinate Dipyrrin−Silicon Complexes. *J. Am. Chem. Soc.* **2011**, *133*, 4726−4729.
(46) Yu, L. H.; Muthukumaran, K.; Sazanovich, I. V.; Kirmaier, C.; Hindin, E.; Diers, J. R.; Boyle, P. D.; Bocian, D. F.; Holten, D.; Lindsey, J. S. Excited-State Energy-Transfer Dynamics in Self-Assembled Triads Composed of Two Porphyrins and an Intervening Bis(dipyrrinato)metal Complex. *Inorg. Chem.* **2003**, *42*, 6629−6647.
(47) Sazanovich, I. V.; Kirmaier, C.; Hindin, E.; Yu, L. H.; Bocian, D. F.; Lindsey, J. S.; Holten, D. Structural Control of the Excited-State Dynamics of Bis(dipyrrinato)zinc Complexes: Self-Assembling Chromophores for Light-Harvesting Architectures. *J. Am. Chem. Soc.* **2004**, *126*, 2664−2665.
(48) Sutton, J. M.; Rogerson, E.; Wilson, C. J.; Sparke, A. E.; Archibald, S. J.; Boyle, R. W. Synthesis and Structural Characterisation of Novel Bimetallic Dipyrromethene Complexes: Rotational Locking of the 5-Aryl Group. *Chem. Commun.* **2004**, 1328−1329.
(49) Thoi, V. S.; Stork, J. R.; Magde, D.; Cohen, S. M. Luminescent Dipyrrinato Complexes of Trivalent Group 13 Metal Ions. *Inorg. Chem.* **2006**, *45*, 10688−10697.
(50) Ikeda, C.; Ueda, S.; Nabeshima, T. Aluminium Complexes of N_2O_2-Type Dipyrrins: The First Hetero-Multinuclear Complexes of Metallo-dipyrrins with High Fluorescence Quantum Yields. *Chem. Commun.* **2009**, 2544−2546.
(51) Kobayashi, J.; Kushida, T.; Kawashima, T. Synthesis and Reversible Control of the Fluorescent Properties of a Divalent Tin Dipyrromethene. *J. Am. Chem. Soc.* **2009**, *131*, 10836.
(52) McRae, E. G.; Kasha, M. *The Molecular Exciton Model*; Academic Press: New York, 1964; pp 23−42.
(53) Kasha, M. Energy Transfer Mechanisms and Molecular Exciton Model for Molecular Aggregates. *Radiat. Res.* **1963**, *20*, 55−70.
(54) Maeda, H.; Hashimoto, T.; Fujii, R.; Hasegawa, M. Dipyrrin Zn-II Complexes with Functional Aryl Groups: Formation, Characterization, and Structures in the Solid State. *J. Nanosci. Nanotechnol.* **2009**, *9*, 240−248.
(55) Telfer, S. G.; McLean, T. M.; Waterland, M. R. Exciton Coupling in Coordination Compounds. *Dalton Transactions* **2011**, *40*, 3097−3108.
(56) Amiri, A.; Comeau, I. M.; Thompson, A. Heteroleptic Zinc Dipyrromethene Complexes. *J. Heterocycl. Chem.* **2006**, *43*, 431−435.
(57) Kee, H. L.; Kirmaier, C.; Yu, L. H.; Thamyongkit, P.; Youngblood, W. J.; Calder, M. E.; Ramos, L.; Noll, B. C.; Bocian, D. F.; Scheidt, W. R.; Birge, R. R.; Lindsey, J. S.; Holten, D. Structural Control of the Photodynamics of Boron−Dipyrrin Complexes. *J. Phys. Chem. B* **2005**, *109*, 20433−20443.
(58) Chibani, S.; Le Guennic, B.; Charaf-Eddin, A.; Laurent, A. D.; Jacquemin, D. Revisiting the Optical Signatures of BODIPY with Ab Initio Tools. *Chem. Sci.* **2013**, *4*, 1950−1963.
(59) Turro, J. N.; Ramamurthy, V.; Scaiano, J. C. *Principles of Molecular Photochemistry: An Introduction*; University Science Book: Sausalito, CA, 2009.
(60) Chibani, S.; Le Guennic, B.; Charaf-Eddin, A.; Laurent, A. D.; Jacquemin, D. Revisiting the Optical Signatures of BODIPY with Ab Initio Tools. *Chem. Sci.* **2013**, *4*, 1950−1963.
(61) Reichardt, C. Solvatochromic Dyes as Solvent Polarity Indicators. *Chem. Rev.* **1994**, *94*, 2319−2358.
(62) Dobkowski, J.; Grabowski, Z. R.; Paeplow, B.; Rettig, W.; Koch, K. H.; Mullen, K.; Lapouyade, R. Intramolecular Charge-Transfer States in Symmetrical Biaryls—The Unusual Case of Biperylenyl. *New J. Chem.* **1994**, *18*, 525−533.
(63) Schneide, F.; Lippert, E. Electron Spectra and Electron Structure of 9,9′-Dianthryl. *Ber. Bunsen-Ges. Phys. Chem.* **1968**, *72*, 1155−1160.
(64) Schneide, F.; Lippert, E. Molecular Calculations for Pi-Electron Structure of 9,9′-Diathryl. *Ber. Bunsen-Ges. Phys. Chem.* **1970**, *74*, 624−630.
(65) Sabatini, R. P.; McCormick, T. M.; Lazarides, T.; Wilson, K. C.; Eisenberg, R.; McCamant, D. W. Intersystem Crossing in Halogenated BODIPY Chromophores Used for Solar Hydrogen Production. *J. Phys. Chem. Lett.* **2011**, *2*, 223−227.
(66) Grozema, F. C.; Swart, M.; Zijlstra, R. W. J.; Piet, J. J.; Siebbeles, L. D. A.; van Duijnen, P. T. QM/MM Study of the Role of the Solvent in the Formation of the Charge Separated Excited State in 9,9′-Bianthryl. *J. Am. Chem. Soc.* **2005**, *127*, 11019−11028.